①

Combustion Systems, Laser Light

APPROVED FOR PUBLIC RELEASE;
DISTRIBUTION UNLIMITED

88 7 18 065

REPORT DOCUMENTATION PAGE

1a. REPORT SECURITY CLASSIFICATION Unclassified	1b. RESTRICTIVE MARKINGS
2a. SECURITY CLASSIFICATION AUTHORITY	3. DISTRIBUTION / AVAILABILITY OF REPORT
2b. DECLASSIFICATION / DOWNGRADING SCHEDULE	Approved for public release; distribution unlimited

4. PERFORMING ORGANIZATION REPORT NUMBER(S) TR-0086A(2060)-3	5. MONITORING ORGANIZATION REPORT NUMBER(S) SD-TR-88-37

6a. NAME OF PERFORMING ORGANIZATION The Aerospace Corporation Laboratory Operations	6b. OFFICE SYMBOL (If applicable)	7a. NAME OF MONITORING ORGANIZATION Space Division
6c. ADDRESS (City, State, and ZIP Code) El Segundo, CA 90245		7b. ADDRESS (City, State, and ZIP Code) Los Angeles Air Force Base Los Angeles, CA 90009-2960

8a. NAME OF FUNDING / SPONSORING ORGANIZATION Air Force Weapons Laboratory	8b. OFFICE SYMBOL (If applicable)	9. PROCUREMENT INSTRUMENT IDENTIFICATION NUMBER F04701-85-C-0086-P00016

8c. ADDRESS (City, State, and ZIP Code) Kirtland Air Force Base, NM 87117	10 SOURCE OF FUNDING NUMBERS			
	PROGRAM ELEMENT NO.	PROJECT NO.	TASK NO.	WORK UNIT ACCESSION NO.

11. TITLE (Include Security Classification)

Particle Sizing in Combustion Systems, Using Scattered Laser Light

12. PERSONAL AUTHOR(S)
Bernard, Jay M.

13a. TYPE OF REPORT	13b. TIME COVERED FROM _____ TO _____	14. DATE OF REPORT (Year, Month, Day) 1988 May 25	15. PAGE COUNT 28

16. SUPPLEMENTARY NOTATION

17. COSATI CODES			18 SUBJECT TERMS (Continue on reverse if necessary and identify by block number)
FIELD	GROUP	SUB-GROUP	particle sizing, holography
			light scattering, laser Doppler spectroscopy

19. ABSTRACT (Continue on reverse if necessary and identify by block number)

Light scattering techniques for particle sizing are reviewed, with emphasis on their use in combustion diagnostics. Submicron soot-particle sizing in flames, using the diffusion-broadened spectrum of scattered light, is discussed in detail, beginning with the pioneering work of S. S. Penner and coworkers. Recent developments in the inversion of scattering data to yield soot number densities and size distributions are then reviewed. Two imaging techniques for measuring particle sizes greater than 1 μm are mentioned: a holographic technique and a method using laser light emitted by the particle itself.

20. DISTRIBUTION / AVAILABILITY OF ABSTRACT [X] UNCLASSIFIED/UNLIMITED ☐ SAME AS RPT. ☐ DTIC USERS	21. ABSTRACT SECURITY CLASSIFICATION Unclassified
22a. NAME OF RESPONSIBLE INDIVIDUAL	22b. TELEPHONE (Include Area Code)	22c OFFICE SYMBOL

DD FORM 1473, 84 MAR   83 APR edition may be used until exhausted.   SECURITY CLASSIFICATION OF THIS PAGE
All other editions are obsolete.

FIGURES

Accesion For

NTIS CRA&I	☑
DTIC TAB	☐
Unannounced	☐
Justification	

By
Distribution /

Availability Codes

| Dist | Avail and/or Special |
| A-1 | |

DTIC
COPY
INSPECTED
6.

3

I. INTRODUCTION

Particle size diagnostics are important in combustion systems that produce and/or consume particles and/or droplets. Production of soot in the burning of hydrocarbons reduces combustion efficiency, and the exhaust of sooting systems is a source of air pollution. Measurement of soot production in flames is therefore crucial for optimizing the efficiency of combustion systems and for reducing their environmental impact. Data that are fundamental to optimizing coal and liquid-fuel combustion systems are the ablation rates of fuel and production rates of soot. Three techniques for obtaining such data are discussed in this report.

Optical diagnostic techniques are especially suited to combustion systems, because chemically reacting flows are more sensitive to the presence of invasive probes than non-reacting flows, and the probes themselves may not survive in the hostile combustion environment. The mapping of velocity distributions in flames[1,2] is an example of a diagnostic situation in which conventional hot-wire velocity probes cannot be readily used but in which use of the laser-Doppler velocimeter (LDV)[3] was successful. Sampling probes for subsequent measurement of particle size in sooting flames are suspected to modify the particle size and even its shape.[4] In situ light scattering techniques avoid such problems and have proven to be useful as combustion diagnostics.

Aerosol particles cover a size range of at least four orders of magnitude. Particles that fall within the first two orders of magnitude, between 10 nm and 1 μm, are typically smaller than the wavelength of the interrogating light. Rayleigh or Mie scattering provides a signal that contains the signature of the scattering particles. These smaller particles undergo significant Brownian motion, which, by the Doppler effect, broadens the (initially narrow) spectrum of the interrogating light as it is scattered by the particle. Measurement of this spectrum to infer particle size is known as diffusion-broadening spectroscopy (DBS). DBS is

reviewed in detail in Section II. Particles in the second two orders of magnitude, between 1 and 100 μm in diameter, are often amenable to photographic imaging techniques. Such direct measurements of particle size are preferred, since, unlike DBS, they do not require knowing the physical and optical parameters of the particles. Holographic imaging is a useful technique in this size range and is discussed in Section III.A. A final imaging technique developed by Chang et al.[5] uses Raman scattering or laser light emitted by the particle itself, and is described in Section III.B.

Many other optical techniques are useful in particle sizing, including extinction and scattering measurements at several angles, wavelengths, or polarizations; the interruption of a focused beam; and LDV measurement of aerodynamic particle diameter. This report emphasizes DBS measurement of particle size because it is a point measurement that can be accomplished in situ in combustion systems. This review also provides a complete summary of the experimental and theoretical considerations that apply to this maturing technology.

II. DIFFUSION-BROADENING SPECTROSCOPY

Soon after the invention of the laser, Forrester[6] discussed the possibility of high-resolution optical spectroscopy using the radar technique of beating the return signal with itself or the signal of a local oscillator. A detector that responds to the square of the electric field (such as a photomultiplier) yields a signal whose power spectrum contains beats between all of the frequencies present in the optical power spectrum. This technique transfers the power spectrum of the scattered light from optical frequencies (10^{15} Hz) to the 0-10 MHz range and is the basis of both LDV and DBS. Many other applications are mentioned in review articles.[7-9]

The use of DBS in flames is reviewed in a recent article by Weill, Lhuissier, and Gouesbet[10] and is summarized here. DBS was first used to size polymer macromolecules in liquid solutions,[11] for which Koppel[12] proposed the method of cumulants to extract information about the particle size distribution. The extension of DBS to aerosol particles was accomplished by Hinds and Reist,[13] who conducted experiments with monodisperse aerosols and suggested detectability (the signal-to-noise ratio at 0 Hz) measurements for polydisperse systems.[14] Edwards et al.[15] discussed the broadening of the measured spectrum when the particles are in a flowing system.

Penner, Bernard, and Jerskey [2,16] applied DBS to soot particle sizing in flames, and measured particle growth on a premixed C_2H_4–O_2 flat flame.[17] Penner and Chang [18] present further experimental results and evidence for the existence of self-preserving particle size distributions in flames, concluding that detectability measurements are not sensitive enough to accurately diagnose log-normal polydispersity, except for selected size ranges using polarized beams.[19] Chang and Penner[20] also derived the effect of turbulence on the measured spectrum and on the ability to measure particle size.

Gouesbet and coworkers[10,21] measured mean diameters and number densities in CH_4-O_2 and $C_3H_8-O_2$ flat flames for various equivalence ratios and flow rates, comparing DBS with particle sizing by optical extinction and scattering measurements. From detailed maps of measured number densities and soot volume fractions, they concluded that coagulation governs particle growth in the region between 0.5 and 2.5 cm above the burner.

King, Sorensen, Lester, and Merklin[22,23] used DBS to measure mean sizes and number densities, and proposed the method of cumulants for polydisperse systems in flames. Taylor, Scrivner, Sorensen, and Merklin[24] theoretically compared the cumulant method with inverse LaPlace transform techniques for diagnosing log-normal polydispersity and concluded that both methods are accurate only if the standard deviation of the particle size distribution is less than 1.4. Recently, those authors[25] used the cumulant technique and measured a decrease in the width of the particle size distribution with height above the burner. They interpreted the decrease as further evidence for the importance of coagulation in the early regions of the flame. A lean flame displayed mostly surface growth after 1.5 cm. Their results also suggest that the self-preserving particle size distribution is attained in these flames.

In the ten years since its first use in flames, DBS has been demonstrated to yield accurate mean particle sizes and number densities for soot. The width of the particle size distribution has also been measured through detailed analysis of the photocurrent correlation function. The limits of flow velocity, turbulence level and scale, and size distribution are well documented, as is the effect of extinction and scattering on the measured parameters. Uncertainties in the flame temperature, viscosity, Knudsen number, and particle refractive index are the main sources of error, but the ability to perform measurements <u>in situ</u> makes DBS the preferred technique for measuring soot particle size in flames.

The theoretical considerations on which the above-described experiments are based are detailed in Section II.A.

A. THEORETICAL BASIS OF DBS

The theory of DBS is based on the broadening of a laser's optical spectrum by the random motion of many diffusing particles, which is analogous to the diffusion broadening of spectral lines. The various particles contribute different Doppler shifts to the light they scatter in the direction of the detector, and the duration of a given signal is interrupted by collisions with the fluid surrounding the particles. The time-averaged detector power spectrum yields the characteristic broadening of the laser light, from which the particle size can be inferred by means of diffusion theory.

The model of a typical laser-scattering experiment is depicted in Fig. 1, which also shows the relation between the wave vectors discussed below. Only homodyne spectroscopy (scattering from a single input beam) is considered here. Note that heterodyne spectroscopy (mixing the homodyne signal with that of another beam) can yield information about the particle velocity (via LDV) as well as its size.[3,16]

Consider a laser beam of frequency ω_0 propagating in the direction of the wave vector $\vec{k}_L$. Light is scattered from this beam (by particles passing through it) into the direction of a photomultiplier, denoted by $\vec{k}_S$. The intersection of the laser beam and the field of view of the photomultiplier defines both the measurement volume and the scattering wave vector: $\vec{k} = \vec{k}_S - \vec{k}_L$. The electric field at the photocathode resulting from scattering by N particles can be written

$$E(t) = \sum_{j=1}^{N} E_j \left[\exp i(\vec{k}\cdot\vec{r}_j(t) - \omega_0 t) \right] \qquad (1)$$

where E_j is the electric field amplitude scattered into the direction of $\vec{k}_S$ by particle j, which is at position $\vec{r}_j$. The intensity of the scattered light is the ensemble average (denoted by $\langle \ \rangle$) of the square of the electric field:
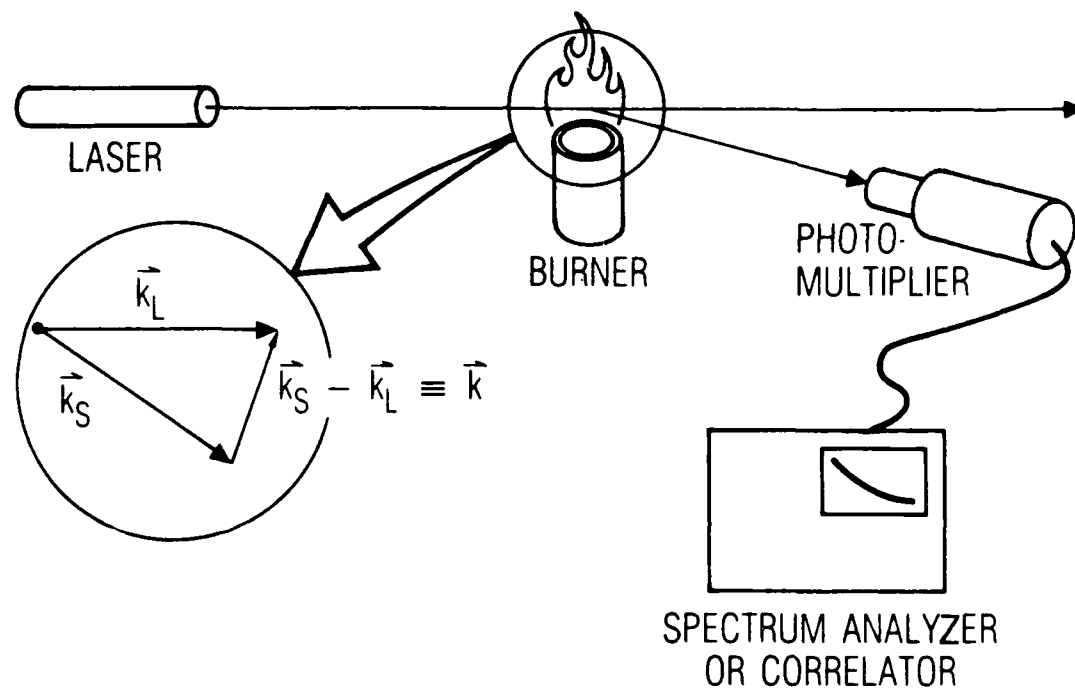
Fig. 1. Schematic diagram of homodyne laser-scattering DBS experiment.

$$I(t) = \langle E^*(t)E(t) \rangle$$

The resulting photocurrent is proportional to the intensity:

$$i(t) = \beta E^*(t)E(t) \tag{2}$$

where β is a detector efficiency ($A\text{-}cm^2\text{-}sec/erg$).

Accounting for the finite relaxation time of the photocathode surface, and assuming that the temporal statistics of the light-scattering events are Gaussian[8] (ensured in dilute particle systems), the photocurrent correlation function can be related to the electric field correlation function by the relation

$$R_i(\tau) = \langle i(t)i(t+\tau) \rangle \tag{3}$$

$$= \beta e I \delta(\tau) + \beta^2 \left[I^2 + \left| R_E(\tau) \right|^2 \right]$$

where e is the electron charge, $\delta(\tau)$ is the Dirac delta function, and

$$R_E(\tau) = \langle E^*(t)E(t+\tau) \rangle \tag{4}$$

is the electric field correlation function.

According to the Wiener-Khinchine theorem, the photocurrent correlation function $R_i(\tau)$ and the photocurrent power spectrum $S_i(\omega)$ are a Fourier transform pair. Thus, from Eq. (3),

$$S_i(\omega) = \frac{1}{\pi} \int_{-\infty}^{\infty} R_i(\tau) \exp(i\omega\tau)\, d\tau$$

$$= \frac{1}{\pi} \beta E I + 2\beta^2 I^2 \delta(\omega) + (\beta^2/\pi) \int_{-\infty}^{\infty} \left| R_E(\tau) \right|^2 \exp(i\omega\tau)\, d\tau \tag{5}$$

The three terms on the right-hand side of Eqs. (3) and (5) are shot noise, the dc component, and the ac term of interest that depends on $R_E(\tau)$, respectively.

11

The electric field correlation function for scattered light from a system of particles carried by a fluid flow must still be derived. Using Eq. (1) in Eq. (4) and noting that the relative positions of neighboring particles are uncorrelated (also ensured in dilute systems), one finds that $R_E(\tau)$ depends on the displacement of individual particles in time τ:

$$R_E(\tau) = \sum_{j=1}^{N} \langle E_j^2 \exp\{ i\vec{k} \cdot [\vec{r}_j(\tau) - \vec{r}_j(0)] - i\omega_0\tau\} \rangle \qquad (6)$$

Equation (6) is a general expression for the electric field correlation function for scattered light from any moving particle. The following subsections derive the resulting photocurrent correlation function and power spectrum for the special case of diffusing particles in flowing systems. The effects of high velocity, turbulence, polydispersity, and short observation times on particle size measurement are derived independently.

1. PURE DIFFUSION, POLYDISPERSE SYSTEMS, LAMINAR FLOW

Displacement due to diffusive motion of the particles enables their size to be inferred. The probability P of diffusive displacement between $\Delta\vec{r}$ and $\Delta\vec{r} + d\Delta\vec{r}$ in time τ is given by the Gaussian random walk

$$P \, d(\Delta\vec{r}_j(\tau)) = (4\pi D_j\tau)^{-1/2} \left[\exp -\frac{|\Delta\vec{r}_j(\tau)|^2}{4D_j\tau} \right] d(\Delta\vec{r}_j(\tau)) \qquad (7)$$

where D_j is the diffusion coefficient for particle j. The relation between particle size and the diffusion coefficient is discussed below. Averaging the diffusive displacements, one obtains

$$R_E(\tau) = \exp(-i\omega_0\tau) \sum_{j=1}^{N} I_j \exp[-(|\vec{k}|^2 D_j - i\vec{k}\cdot\vec{v}_j)\tau] \qquad (8)$$

12

where I_j is the intensity scattered by particle j into the solid angle collected by the detector. In the absence of velocity gradients in the scattering volume, $\vec{v}_j = \vec{v}_k = \vec{v}$, and the particle displacement due to translation is the same for every particle. This Doppler-shifts the optical spectrum by $\vec{k} \cdot \vec{v}$ but does not broaden the spectrum (nor dampen the correlation function). The resulting photocurrent correlation function and power spectrum for purely diffusive motion are (neglecting dc and shot noise)

$$R_i'(\tau) = \frac{\beta^2}{\pi} \sum_{j=1}^{N} \sum_{k=1}^{N} I_j I_k \{ \exp[-|\vec{k}|^2 (D_j + D_k)\tau] \} \tag{9}$$

and

$$S_i'(\omega) = \frac{2\beta^2}{\pi} \sum_{j=1}^{N} \sum_{k=1}^{N} I_j I_k \frac{|\vec{k}|^2(D_j + D_k)}{[|\vec{k}|^2(D_j + D_k)]^2 + \omega^2} \tag{10}$$

respectively. Particle diffusion thus dampens the correlation function of Eq. (9) and broadens the power spectrum of Eq. (10) according to the values of the diffusion coefficients. A mean particle size can be inferred from the half-width of either function, but as these equations show, both functions contain information about the particle size <u>distribution</u> that was responsible for scattering the laser light. Practical considerations are discussed below for the inversion of scattering data to infer both a mean size and the width of an assumed log-normal size distribution.

The particle size distribution determines the range of diffusion coefficients used in the above sums, but, more important, it determines the weight given each contribution via the scattered intensities I_j. Since I_j is typically proportional to the sixth power of the particle radius, the small particles in a wide distribution cannot be measured. Therefore, the practical measurement of log-normal particle size distributions is limited to those with standard deviations less than

13

1.4.[24] In general, for polydisperse systems without velocity gradients, the correlation function is a sum of decaying exponentials,[16,25] and the power spectrum is a sum of Lorentzian contributions.[14,16]

The method of cumulants[12,22] is a convenient data reduction technique that yields the coefficient of the first two terms in the MacLaurin expansion of the sum of decaying exponentials. Comparing measurements of the photocurrent correlation function of light scattered from a flame with Eq. (9), Scrivner and coworkers[25] applied the method of cumulants to determine both the mean particle radius and the width of an assumed log-normal soot particle size distribution. This method fits the entire curve of the measured correlation function to a polynomial expansion in τ. In their experiments, these authors used a digital correlator (commercially available with up to 5×10^8 Hz sampling rates), which efficiently measures $R_i(\tau)$ as the correlation between arrival times of photons at the photocathode. Note that measurements of $S_i(\omega)$ with an appropriate spectrum analyzer contain the same information as measurements of $R_i(\tau)$; many spectrum analyzers compute $S_i(\omega)$ by means of fast-Fourier transformation of the digitally correlated input signal. Fitting the entire curve of the measured power spectrum to theoretical curves based on Eq. (10) is expected to yield accurate particle size distributions. Using only the half-width and detectability of the measured power spectrum has been shown[19] to be inadequate for measuring size distribution, except in a few special cases. The available hardware and software currently favor measuring the correlation function and using the method of cumulants to diagnose reasonably narrow polydispersity in flames.[24]

2. RELATION BETWEEN DIFFUSION COEFFICIENT AND PARTICLE RADIUS

DBS measures the diffusion coefficient D (or the distribution of diffusion coefficients D_j) experimentally. This measurement can be theoretically related to the radius r (or distribution of radii r_j) of the diffusing particles. The elementary diffusion theory used here assumes the particles to be spherical.

Types of diffusion are characterized by the Knudsen number, K_n, the ratio of the gas mean free path to the particle radius:

$$K_n = \frac{\mu}{\rho r} \sqrt{\pi M/RT}$$

where μ is the gas viscosity, ρ is density, M is molecular weight, and T is temperature. For the relatively large particles encountered late in sooting flames, K_n is small and there is Stokes-Einstein diffusion for which

$$D_{Stokes-Einstein} = \frac{k_b T}{6\pi\mu r}$$

where k_b is Boltzmann's constant.

Intermediate Knudsen numbers are often encountered in flames, a regime in which it is appropriate to include the experimentally derived Cunningham slip-correction factor in the above relation:

$$D_{Cunningham} = \frac{k_b T}{6\pi\mu r} \left\{ 1 + K_n \left[A + Q \exp\left(- \frac{b}{K_n}\right) \right] \right\}$$

in which A, Q, and b are of the order 1.2, 0.4, and 1, respectively.[10] Particles smaller than the gas mean free path are known to occur early in sooting flames but have seldom been measured by DBS because of their small scattering coefficient. This regime, which has a large Knudsen number, is known as free-molecular, or Epstein, diffusion, for which

$$D_{Epstein} = \frac{k_b T K_n}{4\pi\mu r}$$

3. PURE DIFFUSION, MONODISPERSE AEROSOL, NO VELOCITY GRADIENTS

Consider a monodisperse aerosol embedded in a laminar flow. The single particle size ensures identical scattered intensities $I_j = I_k$ and diffusion coefficients $D_j = D_k$. In this case, the photocurrent correlation function is a simple exponential and the power spectrum is purely Lorentzian: Eqs. (9) and (10) become

$$R_i'(\tau) = \frac{\beta^2 N^2 I}{\pi} \left\{ \exp\left[-2|\vec{k}|^2 D\tau \right] \right\}$$ (11)

and

$$S_i'(\omega) = \frac{2\beta^2 N^2 I^2}{\pi} \frac{2|\vec{k}|^2 D}{\left[2|\vec{k}|^2 D \right]^2 + \omega^2}$$ (12)

The diffusion coefficient is easily extracted from the half-width of the measured function.[10,15,16] Note that this measurement can be made without knowing the complex index of refraction of the particles, although it must be known for size distribution measurements (in the calculation of I_j and I_k for the given scattering angle).

4.   EFFECT OF PARTICLE TRANSIT TIME (MONODISPERSE SYSTEMS)

If, because of a high enough flow velocity $\vec{v}$, the particle traverses the measurement volume before it can complete several cycles of its Brownian motion, the diffusion coefficient cannot be measured. The particle transit time is taken into account[15,16] by assuming that light is scattered and collected from a spherically symmetric Gaussian intensity distribution with characteristic size σ. With the origin at the center of the scattering volume, the amplitude distribution function of the input laser field is given by

$$A(\vec{r}) = (2\pi\sigma^2)^{-1/4} \exp\left(\frac{-|\vec{r}|^2}{4\sigma^2} \right)$$ (13)

so that instead of Eq. (1), the scattered electric field is

$$E(t) = \sum_{j=1}^{N} E_j \left[\exp i\{\vec{k}\cdot\vec{r}_j(t) - \omega_0 t\} \right] A(\vec{r}_j(t))$$ (14)

Averaging over both diffusive displacement and random particle position gives an electric field correlation function of

$$R_E(\tau) = \exp(-i\omega_0\tau) \sum_{j=1}^{N} I_j \exp\left\{-\left[\frac{|\vec{v}_j|^2\tau^2}{8\sigma^2} + (|\vec{k}|^2 D_j - i\vec{k}\cdot\vec{v}_j)\tau\right]\right\}$$

and modifies the photocurrent correlation function of Eq. (11) to be

$$R_1'(\tau) = \frac{\beta^2 N^2 I^2}{\pi} \exp\left\{-\left[\frac{|\vec{v}|^2}{4\sigma^2}\tau^2 + 2|\vec{k}|^2 D\tau\right]\right\}$$

while the power spectrum of Eq. (12) becomes the Voigt function[16]—the convolution of Gaussian and Lorentzian functions. As discussed in Refs. 15 and 16, the particle transit time places an upper limit on particle sizes that can be measured using a beam size σ in the face of a flow velocity v; particles have measurable diffusion coefficients D if the Voigt parameter z satisfies

$$\text{Re}(z) = \frac{\sigma}{|\vec{v}|}\left(2|\vec{k}|^2 D\right) \geq 0.2$$

In most experiments, $\vec{k}$ and σ have been made large enough to require small transit-time corrections. Transit-time contribution to the power spectrum for polydisperse systems is derived in Ref. 16.

5. EFFECT OF TURBULENCE (INCLUDING TRANSIT TIME, MONODISPERSE SYSTEMS)

As noted by Chang and Penner,[20] if the length scale of turbulence is large compared with the scattering volume, it has no measurable effect on the homodyne power spectrum or correlation function. There is no turbulence effect because, at any instant, there are no velocity gradients in the scattering volume, and the results for diffusion in laminar flow apply.

If its length scale is small, turbulence can produce a random displacement of particles while they are in the measuring volume. The resulting dampening of $R_1(\tau)$ [broadening of $S_1(\omega)$] may impair particle size measurements. Following Ref. 20, the velocity of particle j is separated into mean and fluctuating components:

17

$$\vec{v}_j = \vec{v}_{mean} + \Delta\vec{v}_j$$

An isotropic Gaussian fluctuating velocity distribution is assumed, for which the probability of particle j having a fluctuating component between $\Delta\vec{v}_j$ and $\Delta\vec{v}_j + d\Delta\vec{v}_j$ is

$$P \; d(\Delta\vec{v}_j\tau) = (2\pi v_T^2 \tau^2)^{-3/2} \{ \exp[-|\Delta\vec{v}_j|^2\tau^2/(2v_T^2\tau^2)]\} \; d(\Delta\vec{v}_j\tau)$$

where v_T is the characteristic width of the velocity fluctuation distribution. In calculating the electric field correlation function the ensemble average over turbulent displacement $\Delta\vec{v}_j$ is included with the average over diffusive displacement r, and the average over particle position $\vec{r}$ within the volume defined by $A(\vec{r})$. The result is[20]

$$R_E(\tau) = \exp[i(\vec{k}\cdot\vec{v}-\omega_0)\tau] \sum_{j=1}^{N} I_j[\exp-(|\vec{k}|^2 D_j\tau + \frac{|\vec{k}|^2 v_T^2 \tau^2}{2} + \frac{|\vec{v}_j|^2\tau^2}{8\sigma^2})]$$

The photocurrent correlation function becomes

$$R_i'(\tau) = \frac{\beta^2 N^2 I^2}{\pi} \exp\{-[2|\vec{k}|^2 D\tau + (|\vec{k}|^2 v_T^2 + \frac{v^2}{4\sigma^2})\tau^2]\}$$

and the photocurrent power spectrum is "the convolution of the following three components: a Lorentzian profile due to the Brownian motion, a Gaussian profile due to the turbulent velocity fluctuations, and another Gaussian profile due to the nonuniformity of illumination in the coherence volume."[20] This spectrum is again a Voigt function whose Lorentzian part is still $2K^2D$, but its Gaussian component is now proportional to

$$[4|\vec{k}|^2 v_T^2 + (v^2/\sigma^2)]^{-1/2}$$

The Gaussian component creates an upper limit of particle sizes that can be measured in the face of turbulence, similarly to the upper limit imposed by transit time discussed in the preceding subsection. Mono-disperse particles can be sized if the experimental conditions are such that

$$Re(z) = \frac{2|\vec{k}|^2 D}{\sqrt{4|\vec{k}|^2 v_T^2 + (v^2/\sigma^2)}} \geq 0.2$$

which results in a measurable Lorentzian contribution. Chang and Penner[20] note that, for certain combinations of particle size, measurement volume, and turbulence level, three separate homodyne measurements at different scattering angles can yield v, v_T, and D simultaneously. Heterodyne LDV measurements of v and v_T can always be used to accurately assess the Gaussian contributions and to determine the feasibility of particle size measurement.

6. EFFECT OF SHORT OBSERVATION TIMES

To use DBS for time-dependent particle size measurement, or for measurement using pulsed laser sources, the effect of short observation times must be investigated. This effect is discussed in detail by Penner, Bernard, and Chang.[26] The simplest analysis assumes that the observation time is much shorter than the particle transit time, and that turbulence can be neglected. Here, the scattered electric field is multiplied by a square function $\Pi(t)$ representing the observation time T:

$$\Pi(t;T) = \begin{cases} 1 & \text{for } 0 < t < T \\ 1/2 & \text{for } t = 0 \text{ and } T \\ 0 & \text{for } t > T \end{cases}$$

The autocorrelation of the square function is the triangle function,

$$\Lambda(\tau;T) = \begin{cases} 1 - \tau/T \text{ for } 0 < t < T \\ 1 \text{ for } t = 0 \\ 0 \text{ for } t > T \end{cases}$$

so that the scattered field correlation function for a single particle size becomes

$$R_E(\tau) = NI \ \Lambda(\tau;T) \ \exp(-i\omega_0\tau) \ \exp(-|\vec{k}|^2 D\tau)$$

The photocurrent correlation function is damped by the triangle function squared:

$$R_i(\tau) = \frac{\beta^2 N^2 I^2}{\pi} \left[\Lambda(t;T)\right]^2 \ \exp(-2|\vec{k}|^2 D\tau)$$

and its power spectrum becomes the convolution of the Lorentzian diffusion contribution and the spectrum of the square of the triangle function.[26] The latter contribution is

$$(\frac{2}{\pi\omega^2 T})\{1 - \frac{\sin(\omega T)}{\omega T}\}$$

Experimenters must determine which of the corrections discussed in Subsections 4 through 6 above apply to their DBS measurement (discussed in Subsections 1 and 3), and minimize those corrections over which they have control.

B. SELECTED EXPERIMENTAL RESULTS

DBS has been used to measure soot particle sizes in many types of flames. Studies on flat flames of ethylene, acetylene, methane, and propane, and on wick flames of kerosene and paraffin, appear in published literature.[10] Two recent studies[10,25] are worthy of review here because they demonstrate the maturity of this technique and its utility in elucidating the mechanism of soot growth.

Weill, Lhuissier, and Gouesbet[10] have measured mean particle radii
above a methane-oxygen flat flame using DBS, and have also inferred soot
number densities at each measurement location, based on the scattered
signal strength and the measured particle size. These data were taken as
a function of height above the burner for two fuel/oxygen equivalence
ratios, with three values of the unburned gas velocity at each equivalence
ratio. An interesting result is obtained when the particle size and num-
ber density are plotted as a function of residence time in the flame,
instead of height above the burner: Regardless of the unburned gas veloc-
ity, flames of the same equivalence ratio produce identical soots at iden-
tical times in the flame.[10] This result is expected for a soot growth
mechanism (such as surface growth or coagulation) in which the particle
size depends on the number of collisions it has encountered.

Particle size and number density can be used to calculate the soot
volume fraction at the measurement location. Weill et al. have noted that
if surface growth were responsible for the increase in particle size with
height above the burner, the number density would remain constant as the
soot volume fraction increased, and coagulation of smaller particles would
result in decreasing number density and constant volume fraction. Their
plot of number density versus soot volume fraction is depicted in Fig.
2. For the two flames with higher flow velocity, a nearly constant volume
fraction accompanies the decrease in number density with height above the
burner, suggesting the dominance of coagulation for soot growth in these
flames. Only very late in the faster flames, or throughout the slow
flame, when the number density is well below 10^{+15} m^{-3}, does surface
growth become evident.

Scrivner, Taylor, Sorensen, and Merklin[25] have measured both the mean
particle radius and the width of the soot particle-size distribution as
functions of height above a premixed methane/oxygen flat flame. They fit
the measured correlation function to a second order expansion in τ:
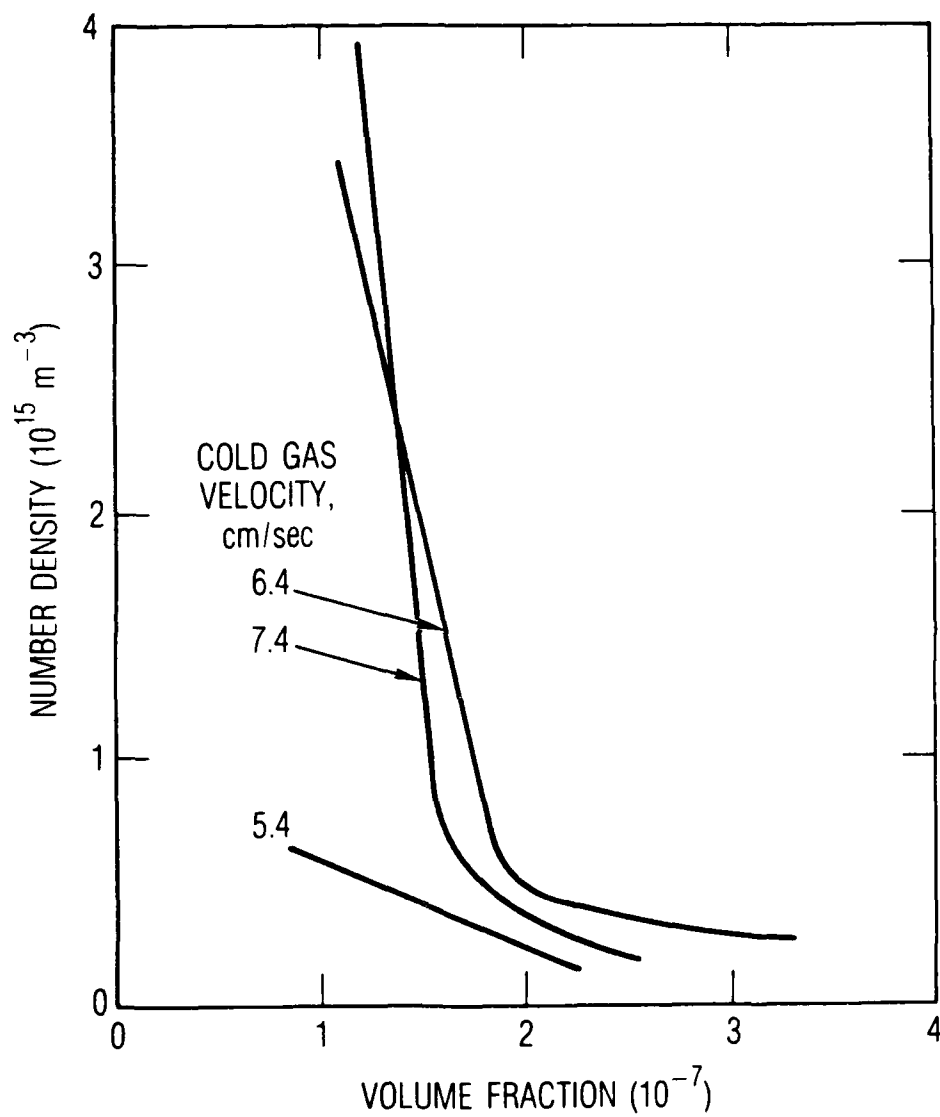
21

Fig. 2. Number density as a function of soot volume fraction for an equivalence ratio of 2.4, at three values of the unburned gas velocity.

$$R_1'(\tau) = C_0 \, \exp(-2K_1\tau + K_2\tau^2)$$

The mean particle radius and the standard deviation of the assumed log-normal particle size distribution were obtained from K_1 and K_2, the first two cumulants in this expansion. Scrivner et al.'s measurements show a decrease in the standard deviation of the distribution with height above the burner, which they interpreted as verifying the dominance of coagulation in soot particle growth. Finally, they quote the theory of diffusion-controlled coagulation (developed by Pich, Friedlander, and Lai[27]), which predicts the narrowing of an initially broad distribution toward the limit of the approximately log-normal self-preserving size distribution. This corroborates the light-scattering and DBS measurements of Chang and Penner[20] that also gave evidence that the self-preserving distribution is attained in sooting flames.

III. IMAGING TECHNIQUES

Particles larger than a few microns are difficult to size by DBS, but can be accurately sized by microscopy or holography. Motion pictures can be made of droplet and particle combustion, and large soots from combustion exhaust can also be photographed. The complicated optical systems required for microscopy, and their small depth of field, can be overcome by holography. Holographic measurement of particle size, shape, and velocity is discussed in Section III.A. In Section III.B are described techniques by which transparent droplets can be made to emit laser light or Raman-scattered light to enable them to be photographed easily.

A. HOLOGRAPHIC PARTICLE DIAGNOSTICS

Like DBS, far-field holography was developed soon after the laser was invented. Its first description[28] and considerable development can be attributed to B. J. Thompson. Far-field holography has become an accepted technique in particle-size analysis and is complementary to DBS: it can measure particles of 1-μm diameter and larger. It can also yield the particle velocity and the cross-sectional shape of the particle. Although like DBS in its conceptual simplicity, such holography involves data reduction that requires careful analysis of the optical and flow characteristics of the experiment.

A schematic diagram of the recording of a far-field hologram is shown in Fig. 3a. A photographic emulsion is illuminated by two samples of a short pulse of laser light. The first sample is a plane wave (a beam whose surfaces of uniform phase are flat) taken from the expanded laser beam, and the second sample is light diffracted from the same beam by particles within the measurement volume. The interference of these two beams in the plane of the emulsion is recorded as a hologram. The hologram is reconstructed, as depicted in Fig. 3b, by being illuminated with a plane wave from a continuous-wave laser. The images of the scattering
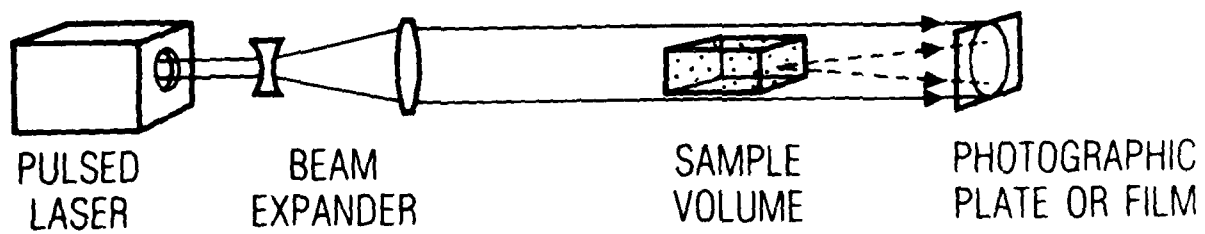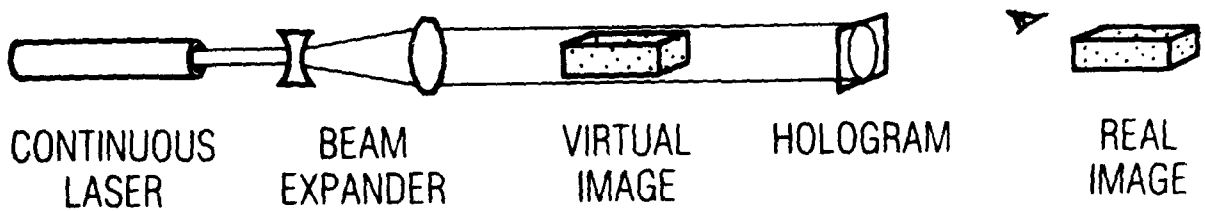
Fig. 3. Schematic description of process for (a) recording a hologram, and (b) reconstructing a hologram.

particles can be studied from the reconstructed hologram or, alternatively, the particles can be sized by direct examination of the interference patterns on the hologram. The practical aspects of this method are reviewed by Cartwright, Dunn, and Thompson,[29] including the required film resolution and format, laser power, coherence, and pulse duration, and the extent to which particle shape can be inferred.

Exposing the hologram with two short pulses enables the particle displacement between pulses to be measured and hence the particle's average velocity during that time. A novel optical data processing technique for such double-exposure holograms is described by Malyak and Thompson.[30] That technique directly yields the velocity distribution within the measurement volume.

B. RAMAN SCATTERING AND LASING DROPLETS

After a light field has been applied to them, transparent droplets or particles (or fibers) can exhibit internal resonances, depending on the particle size and refractive index, and the light wavelength. When such resonances occur when internally reflected light travels an integral number of wavelengths during one round trip inside the droplet, they are known as morphology-dependent resonances. Counterpropagating resonant waves can result in a standing wave inside the droplet with a high intensity near its surface. The droplet surface appears to be highlighted by light scattered from this wave, and photographs of the droplet exhibit clear outlines of its shape. Studied extensively by R. K. Chang and coworkers,[31] the light emitted by the droplet can be elastic scattering, spontaneous Raman scattering, fluorescence, stimulated Raman scattering (up to the fourteenth order), or laser emission. For laser emission to occur, the wave must experience a net gain during one round trip of the droplet. Such a gain was achieved by Chang and coworkers by illuminating rhodamine-doped ethanol droplets with pulses of 532 nm wavelength and observing the dye-laser output at 595 to 600 nm. Notable from their

27

photographs is that the droplets need not be spherical or of a particular size to exhibit laser emission. Indeed, their photographs of highly distorted droplets and liquid streams demonstrate surface lasing to be a powerful technique for highlighting droplets to study their dynamics.

IV. CONCLUSION

Laser diagnostics of particle size have been reviewed, emphasizing their use in combustion systems. For the small particles characteristic of soot in flames, the technique of diffusion-broadening spectroscopy was discussed in detail. This _in situ_ technique has also proven to be applicable to measuring distributions of particle sizes for which the standard deviation is less than 1.45. It has yielded the important conclusion that soot particles coagulate into a self-preserving size distribution within the flame. Two distinctly different laser-based techniques for imaging larger particles were described. These techniques have not yet been applied to combustion systems, but such an application is certainly feasible. Further discussion of the topics covered here is available in the cited references and in their bibliographies.

REFERENCES

1. F. Durst, A. Melling, and J. H. Whitelaw, Comb. Flame 18, 197 (1972).

2. S. S. Penner, J. M. Bernard, and T. Jerskey, Acta Astronaut. 3, 93 (1976).

3. C. P. Wang, "Laser Doppler Velocimetry," J. Quant. Spectrosc. Radiat. Transfer [hereafter JQSRT], 000 (1988).

4. P. H. P. Chang and S. S. Penner, JQSRT 25, 105 (1981).

5. S. X. Qian, J. B. Snow, H. M. Tzeng, and R. K. Chang, Science 231, 486 (1986).

6. A. T. Forrester, J. Opt. Soc. Am. 51, 253 (1961).

7. B. J. Berne and R. Pecora, Annu. Rev. Phys. Chem. 25, 233 (1974).

8. G. B. Benedek, in Polarisation, Matiere et Rayonnement, Presses Universitaires de France, Paris (1969), p. 49.

9. H. Z. Cummins and H. L. Swinney, Prog. Opt. 8, 133 (1970).

10. M. E. Weill, N. Lhuissier, and G. Gouesbet, Appl. Opt. 25, 1676 (1986).

11. R. Pecora, J. Chem Phys. 40, 1604 (1964).

12. D. E. Koppel, J. Chem. Phys. 57, 4814 (1972).

13. W. Hinds and P. C. Reist, Aerosol Sci. 3, 501 (1972).

14. W. Hinds and P. C. Reist, Aerosol Sci. 3, 515 (1972).

15. R. V. Edwards, J. C. Angus, M. J. French, and J. W. Dunning, J. Appl. Phys. 42, 837 (1971).

16. S. S. Penner, J. M. Bernard, and T. Jerskey, Acta Astronaut. 3, 69 (1976).

17. J. M. Bernard and S. S. Penner, Prog. Astronaut. Aeronaut. 53, 411 (1977).

18. S. S. Penner and P. H. P. Chang, in Proceedings, 1979 International Colloquium on Gasdynamics of Explosions and Reactive Systems, AIAA, New York (1981).

31

19. S. S. Penner and P. H. P. Chang, JQSRT 20, 447 (1978).

20. P. H. P. Chang and S. S. Penner, JQSRT 25, 97 (1981).

21. M. E. Weill, P. Flament, and G. Gouesbet, Appl. Opt. 22, 2407 (1983).

22. G. B. King, C. M. Sorensen, T. W. Lester, and J. F. Merklin, in Proceedings, AIAA/ASME 3rd Joint Thermophysics, Fluids, Plasma, and Heat Transfer Conference, AIAA, New York (1982).

23. G. B. King, C. M. Sorensen, T. W. Lester, and J. F. Merklin, Phys. Rev. Lett. 50, 1125 (1983).

24. T. W. Taylor, S. M. Scrivner, C. M. Sorensen, and J. F. Merklin, Appl. Opt. 24, 3713 (1985).

25. S. M. Scrivner, T. W. Taylor, C. M. Sorensen, and J. F. Merklin, Appl. Opt. 25, 291 (1986).

26. S. S. Penner, J. M. Bernard, and P. H. Chang, Physicochemical Hydrodynamics (V. G. Levich Festschrift), Advance Publications Ltd, 30 Craven St., London (1977), pp. 229-246.

27. J. Pich, S. K. Friedlander, and F. S. Lai, Aerosol Sci. 1, 115 (1970).

28. B. J. Thompson, J. Soc. Photo-Opt. Instrum. Eng. 2, 43 (1963).

29. S. L. Cartwright, P. Dunn, and B. J. Thompson, Opt. Eng. 19, 727 (1980).

30. P. H. Malyak and B. J. Thompson, in Particle Sizing and Spray Analysis SPIE Vol. 573, Bellingham, WA (1985), p. 2.

31. J. B. Snow, S. X. Qian, and R. K. Chang, Opt. News 12, 5 (1986).